

Magnetic excitations and exchange interactions in the substituted multiferroics (Nd,Tb)Fe₃(BO₃)₄ revealed by inelastic neutron scattering

I. V. Golosovsky^{1,*}, A. A. Mukhin², V. Skumryev^{3,4}, M. Boehm⁵, W. Schmidt⁵, L.-P. Regnault^{5,6} and I. A. Gudim⁷

¹National Research Center “Kurchatov Institute”, B. P. Konstantinov Petersburg Nuclear Physics Institute, 188300 Gatchina, Russia

²Prokhorov General Physics Institute of the Russian Academy of Sciences, 119991 Moscow, Russia


³Institució Catalana de Recerca i Estudis Avançats (ICREA), E-08010 Barcelona, Spain

⁴Departament de Física, Universitat Autònoma de Barcelona, 08193 Bellaterra, Spain

⁵Institut Laue Langevin, 6 rue Jules Horowitz, BP 156, F-38042 Grenoble, France

⁶Université Grenoble Alpes, CEA, IRIG, MEM-MDN, F-38000 Grenoble, France

⁷Kirenski Institute of Physics, Siberian Division of RAS, 660038 Krasnoyarsk, Russia

 (Received 22 June 2020; revised 28 December 2020; accepted 29 March 2021; published 3 June 2021)

Inelastic neutron scattering spectra in the antiferromagnetic ferrobates Nd_{1-x}Tb_xFe₃(BO₃)₄ ($x = 0, 0.1, 0.2,$ and 1) reveal various magnetic excitations of the interacting iron and rare-earth subsystems. We observe an evolution of the magnetic system from “*easy-plane*”, in the Tb-free ($x = 0$) case, to “*easy-axis*” anisotropy for samples substituted with Tb. The spectra show hybridized Fe and Nd branches, which are determined by the Fe-Nd exchange splitting of the ground-state Nd³⁺ doublet. In the *easy-plane* configuration, near the Brillouin zone center, there are two different pairs of anticrossing quasiacoustic Fe and Nd modes in contrast to the *easy-axis* state, where the two corresponding pairs of the branches are degenerated. The high-energy (exchange) branches are similar in both spin configurations. The Ising-type anisotropy of the Tb ion prevents the magnetic moment from precession. The increasing of the Tb content changes the effective magnetic anisotropy and stabilizes the *easy-axis* state. The spin-wave dispersion in the substituted and pure TbFe₃(BO₃)₄ compounds, which have the same, *easy-axis* magnetic structure, but different crystal symmetry, strongly differ. The observed spectra were analysed in the frame of linear spin-wave theory and the exchange parameters were determined.

DOI: [10.1103/PhysRevB.103.214412](https://doi.org/10.1103/PhysRevB.103.214412)

I. INTRODUCTION

Multiferroic materials with simultaneous magnetic and electric polarization order were discovered in the 1960s [1,2]. Among them, the rare-earth ferrobates RFe₃(BO₃)₄, a class of noncentrosymmetric multiferroics with rhombohedral structure [3–7], have attracted considerable attention, especially in the last decade. The interplay of their magnetic, electric, and optical properties is caused by magnetic exchange interactions between the iron and rare-earth magnetic subsystems. Especially a strong dependence of the electric polarization on application of a magnetic field has been observed, which is of interest for practical applications [8–12].

The strong isotropic Fe-Fe magnetic exchange interaction determines an antiferromagnetic ordering and the Néel temperature. The balance between the rare-earth R-Fe exchange interactions and the single-ion rare-earth anisotropy, as well as the magnetocrystalline anisotropy of the Fe sublattice, are the main additional contributions, which are responsible of the various magnetic properties of the ferrobates. It is of special interest to elucidate the role of the rare-earth ions on the magnetoelectric properties.

There are two types of antiferromagnetic order in the ferrobates: the “*easy-plane*” type, as in NdFe₃(BO₃)₄, with Fe

spins in the basal plane, perpendicular to the trigonal axis, and the “*easy-axis*” type, as in TbFe₃(BO₃)₄, with spins aligned along the trigonal axis. The strong differences in the magnetic structures result from the competition between the Fe and R single-ion anisotropies and R-Fe exchange contribution to the effective magnetic anisotropy, which leads to a complex magnetic structure in the mixed compositions (Nd, Tb)Fe₃(BO₃)₄ [13].

It is important to point out that the spontaneous electric polarization appears only in the *easy-plane* state, although an external magnetic field can induce electrical polarization in the *easy-axis* state as well [14].

The magnetic structure as well as the multiferroic properties are defined by their magnetic exchange parameters J 's, and the magnetic anisotropy, which can be obtained from inelastic neutron scattering by measuring the spin-wave spectra throughout various directions of the Brillouin zone.

The experimental work on spin-wave excitations (or magnons), in multiferroics is extensive, in particular in the classical multiferroics such as BiFeO₃ [15], tungstates MnWO₄ [16,17], and RMnO₃ [18–20]. Concerning ferrobates, only recently spin-wave dispersion in various main symmetry directions of the Brillouin zone in NdFe₃(BO₃)₄ were published [21,22]. Earlier, experimental information on the magnetic excitations was obtained from Terahertz, Raman, AFMR, and infrared spectroscopy [23–27], i.e., only at zero momentum transfer.

*golosovsky_iv@pnpi.nrcki.ru

In the present work on the spin-dynamics in the system $\text{Nd}_{1-x}\text{Tb}_x\text{Fe}_3(\text{BO}_3)_4$, with $x = 0.1$, $x = 0.2$, and $x = 1.0$ [$\text{TbFe}_3(\text{BO}_3)_4$] we continue our previous studies on $\text{NdFe}_3(\text{BO}_3)_4$ [22]. The main objectives here were to trace the evolution of the spin dynamics during the transition from the *easy-plane* to the *easy-axis* magnetic structure, to clarify the specific features of both Nd and Tb ions in the dynamics and to quantify the set of exchange parameters.

II. EXPERIMENT

Large (several mm^3 -size) single crystals of $\text{Nd}_{1-x}\text{Tb}_x\text{Fe}_3(\text{BO}_3)_4$ and $\text{TbFe}_3(\text{BO}_3)_4$ were grown by the solution-melt technique [28] on seeds with a rate not exceeding 1 mm/day. The crystals were enriched with the isotope ^{11}B (not less than 99%) to decrease neutron absorption. The sample quality was verified by single-crystal neutron diffraction [13].

All measurements were performed on the cold triple-axis spectrometers ThALES and IN12 at the Institute Laue-Langevin, France [29]. The spin-dynamics in the sample $\text{Nd}_{0.9}\text{Tb}_{0.1}\text{Fe}_3(\text{BO}_3)_4$ was measured on ThALES. We used a fixed final wave number of $k_f = 1.55 \text{ \AA}^{-1}$ providing the energy resolution of about 0.13 meV FWHM. The scans were performed with a double focusing PG002 monochromator. A velocity selector upstream of the monochromator position of ThALES was used as a broadband neutron filter to suppress higher-order contamination from the monochromator.

The experiments with $\text{Nd}_{0.9}\text{Tb}_{0.1}\text{Fe}_3(\text{BO}_3)_4$ were done at temperature $T = 15 \text{ K}$, where the magnetic order are known to be commensurate, similarly to our previous experiments on $\text{NdFe}_3(\text{BO}_3)_4$ [22]. The inelastic neutron-scattering cross section as a function of moment and energy transfer, $S(Q, E)$, has been measured along the $[\xi \ 0 \ 1.5]$ direction with constant- E scans to energy transfers up to 6 meV.

The sample was mounted inside the so-called ILL-type orange cryostat, providing sample temperatures in the range 1.5–300 K. The crystal was orientated with the reciprocal a^* and c^* axis in the scattering plane of the spectrometers.

The spin-dynamics in the samples $\text{Nd}_{0.8}\text{Tb}_{0.2}\text{Fe}_3(\text{BO}_3)_4$ and $\text{TbFe}_3(\text{BO}_3)_4$ were measured on the cold neutron spectrometer IN12 at 1.5 K with constant- Q scans in the directions $[\xi \ 0 \ 1.5]$ and $[0 \ 0 \ \xi]$ for $\text{Nd}_{0.8}\text{Tb}_{0.2}\text{Fe}_3(\text{BO}_3)_4$ and in the directions $[\xi \ 0 \ 0.5]$ and $[2 \ 0 \ \xi]$ for $\text{TbFe}_3(\text{BO}_3)_4$. A fixed final wave number of $k_f = 1.3 \text{ \AA}^{-1}$ was providing the energy resolution of $\sim 0.08 \text{ meV}$ FWHM.

To study the effects of additional anisotropy, caused by the canting of the antiferromagnetic structure, the spin-wave spectrum was measured in $\text{Nd}_{0.8}\text{Tb}_{0.2}\text{Fe}_3(\text{BO}_3)_4$ under magnetic field of $H = 10 \text{ T}$, applied perpendicularly to the c axis. A cryomagnet with a vertical field was used.

III. FEATURES OF THE MAGNETIC AND CRYSTAL STRUCTURES

$\text{Nd}_{1-x}\text{Tb}_x\text{Fe}_3(\text{BO}_3)_4$ with $x = 0.1$ and $x = 0.2$, as well as the pure compound $\text{NdFe}_3(\text{BO}_3)_4$, have the noncentrosymmetric space group (SG) $R32$ [13,30,31] at low temperatures, while $\text{TbFe}_3(\text{BO}_3)_4$ has the lower symmetric SG $P3_121$ [32,33].

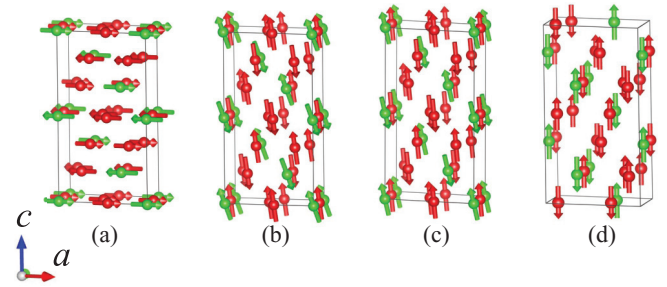


FIG. 1. Magnetic structures of (a) $\text{NdFe}_3(\text{BO}_3)_4$, (b) $\text{Nd}_{0.9}\text{Tb}_{0.1}\text{Fe}_3(\text{BO}_3)_4$, (c) $\text{Nd}_{0.8}\text{Tb}_{0.2}\text{Fe}_3(\text{BO}_3)_4$, and (d) $\text{TbFe}_3(\text{BO}_3)_4$. The magnetic moments of the rare-earth and Fe ions are shown in green and red color, respectively. The magnetic unit cell, which is twice the chemical one, is shown.

In the SG $R32$, three Fe atoms occupy the 9d Wyckoff site with coordinates $(0, x, 0)$, $(-x, -x, 0)$, and $(x, 0, 0)$ in the hexagonal setting, while the rare-earth atom occupies the 3a site with coordinate $(0, 0, 0)$. The atomic positions in the chemical cell multiply by the trigonal translations: $(0, 0, 0)$, $(2/3, 1/3, 1/3)$, and $(1/3, 2/3, 2/3)$. Keeping in mind these translations, there are 12 magnetic atoms in the chemical cell. Because the magnetic cell is twice the chemical cell, there are 24 magnetic moments, providing, in principle, 24 different dispersion branches. However, $2/3$ of the branches have zero inelastic neutron-scattering cross section.

The diagonalization of the dynamic matrix gives four two-fold degenerate branches with nonzero spectral weight. The 24 branches can be constructed from these four branches, using the translations $(1 \ 0 \ 0)$ and $(2 \ 0 \ 0)$ [or $(0 \ 1 \ 0)$ and $(0 \ 2 \ 0)$] in the Q -space [22].

The crystal structure of $\text{TbFe}_3(\text{BO}_3)_4$ is more complicated. In the SG $P3_121$, the Tb atoms occupy the Wyckoff positions 3a with coordinates $(x, 0, 1/3)$, $(0, x, 2/3)$ and $(-x, -x, 0)$. There are two nonequivalent positions for the Fe atoms: the 3a site and the 6c site with coordinates (x, y, z) , $(-y, x - y, z + 1/3)$, $(-x + y, -x, z + 2/3)$, $(y, x, -z)$, $(x - y, -y, -z + 2/3)$, $(-x, -x + y, -z + 1/3)$. There are 12 atoms in the chemical cell, as in the SG $R32$. Again, the magnetic unit cell is twice the chemical cell resulting in 24 nonequivalent magnetic moments, which provide 12 two-fold degenerate branches. In contrast to SG $R32$, all of them have nonzero spectral weight.

The studied substituted compounds $\text{Nd}_{1-x}\text{Tb}_x\text{Fe}_3(\text{BO}_3)_4$ have a magnetic structure close to the *easy-axis* type with a magnetic propagation vector $\mathbf{k} = [0 \ 0 \ 3/2]$, which is typical for compounds crystallized in the SG $R32$ [30,31,34]. In the ground state a complicated, commensurate magnetic structure was found [13].

In contrast with the pure Nd and the substituted ferrobates, $\text{TbFe}_3(\text{BO}_3)_4$ has at low temperatures the *easy-axis* type magnetic order with a propagation vector $\mathbf{k} = [0 \ 0 \ 1/2]$ [33,35]. The magnetic structures are shown in Fig. 1.

IV. MODEL CALCULATIONS

For the numerical calculations of the spin-dynamics studies we used the SpinW software package [36], which

calculates the dispersion curves, $\hbar\omega = E(\vec{Q})$, and their spectral weights, $S(\vec{Q}, E)$, using the classical linear spin-wave approach [37–39]. The Hamiltonian used in SpinW package has the form

$$\begin{aligned}
 H = & \sum_{i,j} J_{Fe-Fe}^{i,j} \vec{S}_i \cdot \vec{S}_j + \sum_{i,j} J_{Fe-R}^{i,j} \vec{S}_i \cdot \vec{s}_j \\
 & + \sum_i [D_{\perp} \cdot (S_{ix}^2 + S_{iy}^2) + D_{\parallel} \cdot S_{iz}^2] \\
 & + \mu_B \cdot \vec{B} \sum_i g_i^{Fe} \cdot \vec{S}_i + \mu_B \cdot \vec{B} \sum_i g_i^R \cdot \vec{s}_i. \quad (1)
 \end{aligned}$$

Here, \vec{S}_i and \vec{s}_j are the effective spin operators of Fe^{3+} and R^{3+} in the Fe and R sublattices, respectively. J_{Fe-Fe} and J_{Fe-R} are the exchange parameters, describing the coupling between the Fe spins and the rare-earth moments. D_{\perp} and D_{\parallel} are the effective anisotropy parameters for the Fe ions, B is an external magnetic field and g_i^{Fe} and g_i^R are the corresponding g tensors. In Eq. (1) positive exchange parameters correspond to antiferromagnetic interactions, while the negative exchange parameters correspond to ferromagnetic interactions.

The effective spin operator s_j^m of the Nd^{3+} moments in the ground state (Kramers doublet) is $1/2$. Because the spin-dynamics measurements of $Nd_{0.9}Tb_{0.1}Fe_3(BO_3)_4$ were performed at the finite temperature of 15 K, the static average spin moment, evaluated from elastic neutron diffraction, $s_j^m = 0.25$ was used [13] in the calculations. In the elastic neutron diffraction experiments, the Fe magnetic moment was found to be $\sim 4 \mu_B$. Therefore, for the substituted compounds, an effective spin of Fe^{3+} $S_i^m = 2.0$ was used.

The ground state of the non-Kramers Tb^{3+} ion in a crystal field is a quasi-doublet (i.e., two close singlets) having its *easy-axis* practically parallel to the c axis. Thus, it can only be split by the c component of the exchange or applied magnetic field. For this reason we considered the Tb^{3+} ions as Ising-type at low temperatures [14,23,26]. The strong anisotropy of the exchange Tb-Fe splitting of the ground Tb^{3+} quasidoublet stabilizes the alignment of Fe spins along the c axis. This induces a change of the magnetic structure from *easy-plane* in the $NdFe_3(BO_3)_4$ to *easy-axis* in the slightly Tb-doped ($x = 0.1$ and $x = 0.2$) compounds.

The Tb^{3+} magnetic moments do not contribute to the spin-wave dynamics. In the vicinity of the frequencies, corresponding to the quasidoublet exchange splitting, Tb^{3+} spin components perpendicular to the c axis are practically absent, as there is no spin precession [14,23]. For this reason we consider the effect of Tb ion substitution only as a source of additional anisotropy energy in the Fe subsystem, which is accounted for as an effective anisotropy constant in Eq. (1).

Exchange interactions depend not only on the distances but on bonds geometry. It is known that in alumborates, (i.e., without Fe sublattice), which possess a similar crystal structure and similar exchange geometry the magnetic order in the rare-earth lattice appears at very low temperatures, for example, $TbAl_3(BO_3)_4$ [40], indicates very weak exchange. It is a reason why we can neglect the interactions in the rare-earth sublattice.

For the SpinW calculation we used the known lattice parameters for $Nd_{1-x}Tb_xFe_3(BO_3)_4$ [30,31] and for pure $TbFe_3(BO_3)$ [33].

V. RESULTS

A. Spin-wave dynamics in the substituted system

$Nd_{1-x}Tb_xFe_3(BO_3)_4$ with SG R32

The inelastic neutron scattering spectra in the substituted ferrobates $Nd_{1-x}Tb_xFe_3(BO_3)_4$ ($x = 0.1$ and 0.2) reveal a manifold of magnetic excitations (Fig. 2). The acoustic branches above 1.5 meV and optical branches between ~ 3 –6 meV could be associated with the Fe-system, while the dispersionless branch around 1 meV is associated with the Nd-subsystem.

For the adequate description of all branches in terms of position and intensity, especially at high energies, a large number of coordination spheres has to be considered. For the $Nd_{1-x}Tb_xFe_3(BO_3)_4$ compounds we limited the magnetic interactions to 12 coordination spheres. Considering more spheres did not affect the spin-wave spectra.

The spin-wave spectra of $Nd_{0.8}Tb_{0.2}Fe_3(BO_3)_4$ were measured at the temperature of 1.5 K with constant- Q scans along the $[\xi 0 1.5]$ and $[0 0 \xi]$ directions, while the spin-wave spectra of $Nd_{0.9}Tb_{0.1}Fe_3(BO_3)_4$ were measured at the temperature of 15 K with constant- E scans along the $[\xi 0 1.5]$ direction only. The observed and calculated spin-wave spectra of $Nd_{1-x}Tb_xFe_3(BO_3)_4$ are shown in Fig. 2. To remove the irrelevant details the experimental plots in Fig. 2 are shown after small smoothing. The initial plots without smoothing are shown in the Supplemental Material [41].

Because of a strong correlation between the large number of variables in our case, the standard refinement implemented into the SpinW package, based on a search of the minimum in the χ^2 residual, did not work properly. Therefore, we sequentially varied the exchange parameters with a small step, searching for the best agreement between the calculated and the observed magnon positions. As well we accounted for the best consistency between the calculated and the measured spin-wave dispersion maps, i.e., magnon intensities. Following this procedure, we used as few independent parameters as possible.

In the scan deconvolution, to refine the positions of the magnetic excitations, we used a Voigtian shape-line, i.e., convolution of the Gaussian and Lorentzian.

For comparison, we also show the spectra of $NdFe_3(BO_3)_4$ with the same SG R32, but with the *easy-plane* magnetic structure. These spectra were recalculated using early published data [22]. Here, we added an additional coordination sphere at the distance of 6.217 Å to check for consistency with the calculations for the substituted compounds.

In the SG R32 with propagation vector $\mathbf{k} = [0 0 3/2]$ the magnetic zone center is at $(0, 0, 1.5)$. In magnetic neutron diffraction, only spin components perpendicular to the scattering vector Q have finite intensities. Therefore, for the *easy-axis* magnetic structure, with moments aligned along the c axis, the reflection $(0, 0, 1.5)$ should be absent. The observed weak elastic intensity at this point results from small in-plane

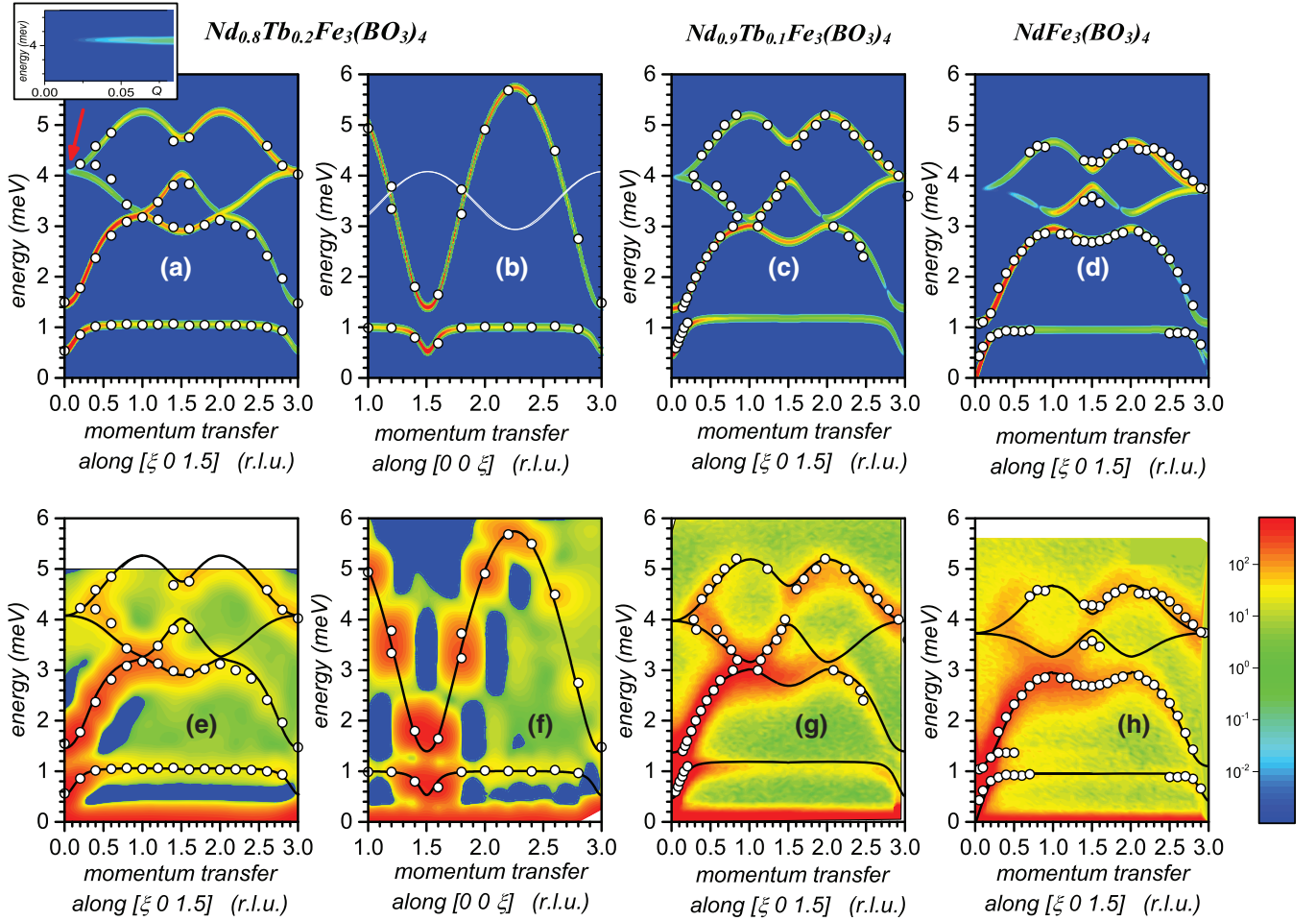


FIG. 2. Calculated [(a)–(d)] and observed [(e)–(h)] maps of spin-wave dispersion in the substituted compounds $\text{Nd}_{1-x}\text{Tb}_x\text{Fe}_3(\text{BO}_3)_4$ and $\text{NdFe}_3(\text{BO}_3)_4$. [(a), (b)] and [(e), (f)] Maps of $\text{Nd}_{0.8}\text{Tb}_{0.2}\text{Fe}_3(\text{BO}_3)_4$, measured along $[\xi 0 1.5]$ and $[0 0 \xi]$ directions, respectively. Maps of $\text{Nd}_{0.9}\text{Tb}_{0.1}\text{Fe}_3(\text{BO}_3)_4$ measured along the $[\xi 0 1.5]$ direction [(c), (g)] and maps of $\text{NdFe}_3(\text{BO}_3)_4$ measured along the $[\xi 0 1.5]$ direction [(d), (h)] [22] are shown for comparison. The calculated dispersion curves $\hbar\omega = E(\vec{Q})$ are shown as well in the observed maps of spin-wave dispersion, panels [(e)–(h)]. White open circles correspond to the magnon positions, obtained after deconvolution of the measured energy scans for Voigtians. Only branches with nonzero inelastic neutron-scattering cross section are shown, apart from the panel (b), where a branch with zero inelastic neutron-scattering cross section is shown by a white line (see text). The spin-wave dispersion in $\text{Nd}_{0.8}\text{Tb}_{0.2}\text{Fe}_3(\text{BO}_3)_4$ (e) was measured with a step size of $\Delta Q = 0.05$ reciprocal lattice units (r.l.u.), while in the map (f) $\Delta Q = 0.1$ r.l.u. The weak dispersion-less branch in the panel (h) around 1.4 meV is associated with the transition inside the Nd^{3+} doublet [22]. Scales are logarithmic.

components of the magnetic moments, which allowed us to measure the transverse polarized spin-waves close to the elastic line.

B. Spin-wave dynamics in $\text{Nd}_{0.8}\text{Tb}_{0.2}\text{Fe}_3(\text{BO}_3)_4$ in applied magnetic field

Applying a magnetic field perpendicular to the moments, aligned along the c axis, causes a canting of the antiferromagnetic sublattices and the appearance of a weak ferromagnetic moment, which strongly affects the spin-wave dynamics. Because the Nd moments are coupled to the strong exchange field of the Fe sublattice, the tilt and the resulting net ferromagnetic moment, should be defined by a self-consistent procedure.

Our measurements of $\text{TbFe}_3(\text{BO}_3)_4$ in a magnetic field up to 9 T, applied perpendicularly to the c axis, showed a linear dependence of the magnetization in the field. Therefore,

we supposed that the Tb moments remain aligned along the c axis, and only Fe and Nd moments tilt away from the c axis. Second, we took into account the known g factors of the ground doublet Nd^{3+} ion [23,26]. Third, we fixed the exchange parameters to the values, refined from the spin-wave spectra in zero magnetic field. Finally, from our neutron diffraction experiments at 2 K, it followed that the magnitude of the Fe spins only weakly depends on the field. Therefore, we used the fixed values of the magnetic moments, refined from these experiments.

With the help of the SpinW package, we calculated the ground state energy $E(\Theta_{\text{Nd}}, \Theta_{\text{Fe}})$ as a function of the deviation angles Θ_{Nd} and Θ_{Fe} to find the equilibrium state in the magnetic field. The azimuthal angle in the basic plane was fixed to 139.0° , which corresponds to the magnetic field direction $[-1 2 0]$.

The calculations indicate a minimum at the angles $\Theta_{\text{Nd}} = 40^\circ$ and $\Theta_{\text{Fe}} = 8^\circ$. These angles correspond to net

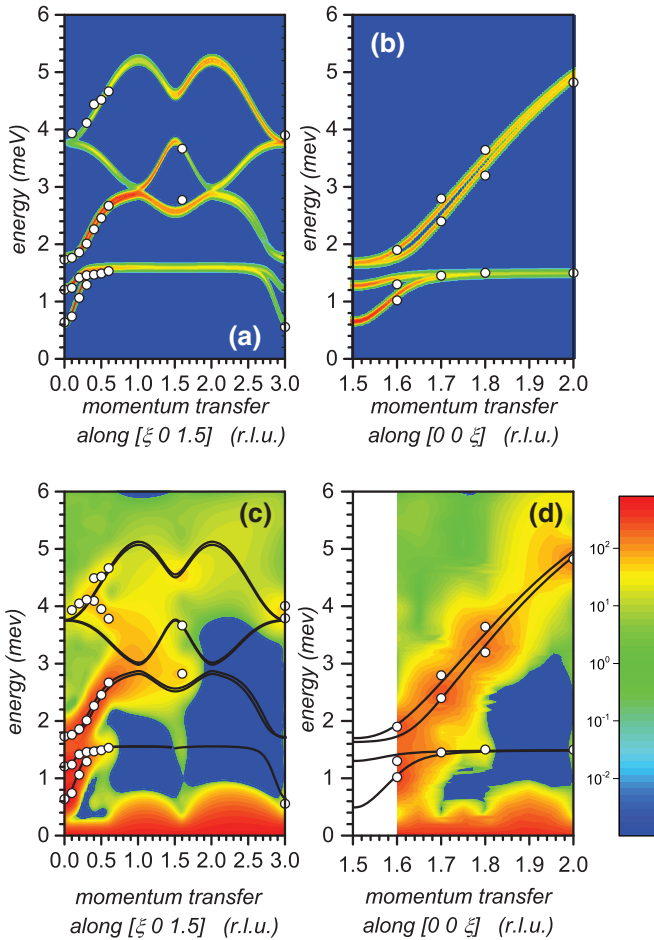


FIG. 3. Calculated [(a), (b)] and observed [(c), (d)] maps of spin-wave dispersion for $\text{Nd}_{0.8}\text{Tb}_{0.2}\text{Fe}_3(\text{BO}_3)_4$ along $[\xi 0 1.5]$ and $[0 0 \xi]$ directions in an applied magnetic field of 10 T at a temperature of 1.5 K. The calculated dispersion curves $\hbar\omega = E(\vec{Q})$ are shown as well in the observed maps of spin-wave dispersion, panels (c) and (d). White open circles correspond to the magnon positions, obtained after deconvolution of the measured energy scans for Voigtians. Scales are logarithmic.

ferromagnetic moments of $0.77 \mu_B$ and $0.42 \mu_B$ for Nd^{3+} and Fe^{3+} ion, respectively.

Using the refined exchange parameters and the magnetic structure found in the ground state, an excellent agreement between the calculated spin-wave spectra and the observed one was obtained (Fig. 3).

It should be noted that the deviation angles Θ_{Nd} and Θ_{Fe} could be refined from the observed spectra by fixing the values of the magnetic moments, i.e., by the inverse procedure.

C. Spin-wave dynamics in the “easy-axis” antiferromagnetic $\text{TbFe}_3(\text{BO}_3)_4$ with SG $P3_121$

Unlike the substituted compounds crystallizing in the SG $R32$, $\text{TbFe}_3(\text{BO}_3)_4$ crystallizes in the lower SG $P3_121$, with two nonequivalent positions of the Fe atoms. As it was mentioned above, Tb does not participate in the spin-wave dynamics. Therefore, only the Fe sublattice was considered in the calculation. There are nine double-degenerated branches

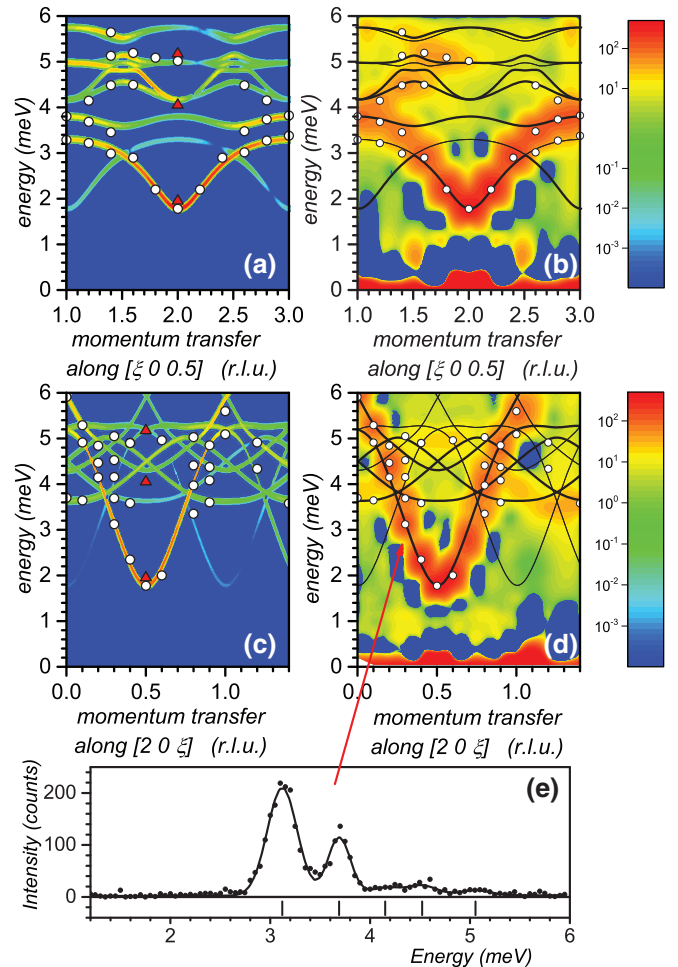


FIG. 4. Calculated [(a), (c)] and observed [(b), (d)] spin-wave spectra for $\text{TbFe}_3(\text{BO}_3)_4$ measured at 1.5 K with const- Q scans in the directions $[\xi 0 0.5]$ and $[2 0 \xi]$ around the magnetic reflection $(2 0 0.5)$. The calculated dispersion curves $\hbar\omega = E(\vec{Q})$ are shown as well in the observed maps of spin-wave dispersion. White open circles correspond to the magnon positions, obtained after deconvolution of the measured energy scans for Voigtians. Red triangles are experimental data from THz-spectroscopy experiments [23,42]. (e) The profiles of measured and calculated energy scans at $Q = [2 0 0.3]$. Vertical bars indicate the magnon positions. Scales are logarithmic.

in the spin-dynamics spectrum, all of them have nonzero spectral weight.

For the adequate description of the upper high-energy branches, it was necessary to consider up to 17 coordination spheres with a radius up to 7.1 \AA . To reduce the number of parameters we neglected the differences in the exchange parameters in the distant spheres, as in the case of the substituted ferrobates $\text{Nd}_{1-x}\text{Tb}_x\text{Fe}_3(\text{BO}_3)_4$. We also supposed that the values of the Fe spins in both crystallographic positions are equal. Under these assumptions, nine refined exchange parameters and one uniaxial anisotropy parameter remain.

The calculated and observed spin-wave spectra of $\text{TbFe}_3(\text{BO}_3)_4$, measured along the $[\xi 0 0.5]$ and $[2 0 \xi]$ directions, around the magnetic reflection $(2, 0, 0.5)$ are shown in Fig. 4.

TABLE I. Refined exchange parameters for $\text{Nd}_{1-x}\text{Tb}_x\text{Fe}_3(\text{BO}_3)_4$ (meV)^a.

	Spheres	Interaction	Distance (Å)	$\text{Nd}_{0.8}\text{Tb}_{0.2}\text{Fe}_3(\text{BO}_3)_4$	$\text{Nd}_{0.9}\text{Tb}_{0.1}\text{Fe}_3(\text{BO}_3)_4$	$\text{NdFe}_3(\text{BO}_3)_4$
J_1	1	Fe-Fe intrachain	3.191	0.71	0.71	0.71
J_3	2	Fe-Nd interchain	3.785	0.07	0.08	0.04
J_4	3	Fe-Nd in-plane	4.317	-0.03	-0.05	-0.05
J_2	4	Fe-Fe in-plane	4.403	0.15	0.15	0.21
J_5	5	Fe-Fe interchain	4.868	0.14	0.14	0.095
J_6	7	Fe-Fe intrachain	5.427	-0.06	-0.07	-0.05
J_8	10,11	Fe-Fe interchain	6.091	0.10	0.10	0.12
J_9	12	Fe-Fe interchain	6.217	-0.08	-0.09	-0.10
anisotropy parameters						
				D_{\parallel}	D_{\parallel}	D_{\perp}
uniaxial anisotropy				-0.015	-0.015	0.0
“in-plane” anisotropy				0.0	0.0	-0.007

^aThe estimated error of the exchange parameters is about 0.01 meV, for the single-ion anisotropy terms it is ~ 0.002 meV.

VI. DISCUSSION

The refined exchange parameters for the substituted compounds $\text{Nd}_{1-x}\text{Tb}_x\text{Fe}_3(\text{BO}_3)_4$ with *easy-axis* magnetic structure are presented in Table I. For comparison, the exchange parameters of $\text{NdFe}_3(\text{BO}_3)_4$ with the same crystal symmetry, but with *easy-plane* magnetic structure, are shown as well.

The single-ion anisotropy in the *easy-plane* magnetic structure is described by a matrix with the diagonal terms: $D_{xx} = D_{yy} = D_{\perp} \neq 0$ and $D_{zz} = D_{\parallel} = 0$, while in the *easy-axis* case $D_{\perp} = 0$ and $D_{\parallel} \neq 0$. They are shown in Table I as well.

The spin-wave dispersion in $\text{Nd}_{1-x}\text{Tb}_x\text{Fe}_3(\text{BO}_3)_4$ and $\text{NdFe}_3(\text{BO}_3)_4$ with *easy-axis* and *easy-plane* structure, respectively, look similar, apart from near the center zone, at $Q = [0\ 0\ 1.5]$ (Fig. 2). While in the *easy-plane* compound $\text{NdFe}_3(\text{BO}_3)_4$ there are two nonresolved branches at low energies, one of them is without gap [22], in the substituted *easy-axis* compounds these branches are degenerate and a gapless branch is absent. The observed “branch repulsion” is caused by the hybridization of the Nd and Fe excitations, i.e., electron transitions between the ground Nd-doublet and the quasiaoustic Fe spin branches.

The similarity of the spin-wave dynamics is an expected result and stems from the invariance of the isotropic exchange Hamiltonian relative to the rotation of all spins as a whole, when the contributions from the single-ion anisotropy and the anisotropic exchange are small.

The application of a magnetic field of 10 T, perpendicular to the spin direction in the *easy-axis* compound $\text{Nd}_{0.8}\text{Tb}_{0.2}\text{Fe}_3(\text{BO}_3)_4$, results in a canting of the axial antiferromagnetic structure, which removes the degeneracy of the branches in the spin-wave spectra (Fig. 3). It is seen that the magnetic field leads to a splitting of the degenerated hybridized Nd-Fe branch and increases the energy gap.

In $\text{TbFe}_3(\text{BO}_3)_4$ and $\text{Nd}_{1-x}\text{Tb}_x\text{Fe}_3(\text{BO}_3)_4$, compounds with similar *easy-axis* magnetic structure but with different crystal symmetry (SG $P3_121$, and SG $R32$, respectively), the spin-wave dispersion strongly differ (Figs. 2 and 4). The low-energy branch at ~ 1 meV is only observed in the substituted compounds, where the Fe-Nd interaction exists.

The analysis shows a strong dependence of the spin-wave dynamics on the directions in the crystal. There are intense high-energy branches above ~ 3.2 meV along the $[\xi\ 0\ 1.5]$ direction [Figs. 2(a) and 2(e)], while they are invisible along the $[0\ 0\ \xi]$ direction [Figs. 2(b) and 2(f)].

The calculation shows that the intensity of these high-energy branches along the $[\xi\ 0\ 1.5]$ direction falls very quickly to zero when approaching the point (0 0 1.5) (zone center), as shown in the insert in Fig. 2(a). The corresponding branches along the $[0\ 0\ \xi]$ direction have a zero inelastic neutron-scattering cross section in the frame of the Hamiltonian used [white line in Fig. 2(b)]. Such strong anisotropy was observed in all substituted compounds, regardless of their magnetic structure, *easy-plane* or *easy-axis*.

TABLE II. Refined exchange parameters for $\text{TbFe}_3(\text{BO}_3)_4$ (meV)^a.

	Spheres	Interaction	Distance (Å)	$\text{TbFe}_3(\text{BO}_3)_4$
J_{11}	1	Fe1-Fe1 intrachain	3.177	0.97
J_{12}	2	Fe2-Fe2 intrachain	3.188	0.93
J_{21}	3	Fe1-Fe2 interchain	4.343	0.25
J_{22}	4	Fe2-Fe2 interchain	4.411	0.23
J_5	5-7	Fe1-Fe1, Fe2-Fe2 in plane	4.821–4.849	0.15
J_6	8-9	Fe1-Fe1, Fe2-Fe2 intrachain	5.402–5.408	0.04
J_9	17	Fe2-Fe1 interchain	6.23	0.10
J_{10}	12	Fe-Fe interchain	7.107	0.08
effective uniaxial anisotropy $D_{\parallel} = -0.04$				

^aThe estimated error of the exchange parameters is about 0.01 meV for the anisotropy term ~ 0.002 meV.

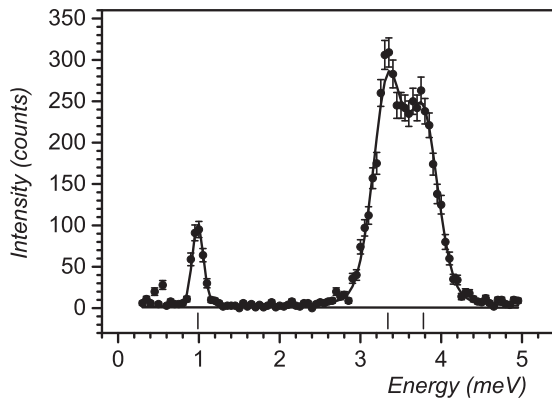


FIG. 5. The energy scan measured at $Q = [0\ 0\ 1.2]$ - for $\text{Nd}_{0.8}\text{Tb}_{0.2}\text{Fe}_3(\text{BO}_3)_4$. The peaks are approximated by the Voigtian line-shape with the same FWHM. Vertical bars indicate the magnon positions at 3.34(1) meV and 3.78(1) meV.

In the spin-wave spectra of $\text{Nd}_{0.8}\text{Tb}_{0.2}\text{Fe}_3(\text{BO}_3)_4$, measured along $[0\ 0\ \xi]$ two magnons at the same momentum transfer $Q = [0\ 0\ 1.2]$ (or at $Q = [0\ 0\ 1.8]$), but with different energies are seen. The corresponding profile is shown in Fig. 5.

However, only one spin-wave branch with nonzero intensity passes through those points [Figs. 2(b) and 2(f)]. Remarkably, the high-energy peak appears close to the branch with nominally zero spectral weight [shown in Fig. 2(b) by a white line]. We suppose that this double peak could be associated with the transfer of intensity in the anticrossing region at the intersection of two branches—an intense branch and a branch with a nominally zero intensity, due to a weak anisotropic exchange.

Unfortunately, to evaluate reliably a weak anisotropic exchange interaction from the measured spin-dynamic spectra is impossible in the frame of our experimental accuracy and the used expansive model with many parameters. The contribution of the anisotropic Fe-Fe exchange interactions, although expected to be small compared to the isotropic one, requires a special, more detailed study, which is beyond the scope of our paper.

Since the interatoms distances in the compounds with a similar crystal symmetry (SG *R32*) are close, the exchange parameters for the *easy-plane* compound $\text{NdFe}_3(\text{BO}_3)_4$ and the *easy-axis* compound $(\text{Nd}, \text{Tb})\text{Fe}_3(\text{BO}_3)_4$ are practically identical, apart from the Fe-Nd exchange parameter J_3 (see Table I). The refined exchange parameters for $\text{TbFe}_3(\text{BO}_3)_4$ with SG *P3₁21* are presented in Table II.

Some exchange parameters, e.g. J_5 [the 5th coordination sphere with a radius of 4.87 Å in $\text{Nd}_{1-x}\text{Tb}_x\text{Fe}_3(\text{BO}_3)_4$] or the exchange parameters J_6 and J_8 , (8 and 13 coordination spheres at the distances 5.40 Å and 6.06 Å, respectively) in $\text{TbFe}_3(\text{BO}_3)_4$, which couple the parallel spins, appeared to be positive, i.e., correspond to antiferromagnetic coupling. As the magnetic structure in these complex systems results from many competing super-exchange interactions, there is no simple connection between the sign of the exchange integral and the corresponding magnetic moment direction.

The super-exchange interactions depend on the overlapping of orbitals, known as the Kanamori-Goodenough rules

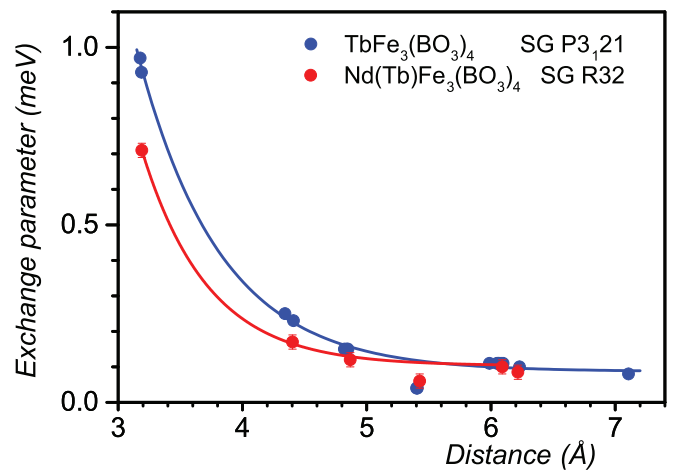


FIG. 6. Dependence of the refined absolute value of the exchange parameters on the distance for $(\text{Nd}, \text{Tb})\text{Fe}_3(\text{BO}_3)_4$ (in red) and $\text{TbFe}_3(\text{BO}_3)_4$ (in blue). The lines are guide-to-the-eyes and correspond to a fit with exponential decay. The error does not exceed the symbol size.

[43]. The analysis of the exchange parameters demonstrates the complex interplay between the distance and the exchange interaction pathway.

A large number of the exchange parameters for different coordination spheres refined from spin-wave spectra allow us to trace the dependence of the exchange parameter on the distance in the Fe subsystem (Fig. 6). Surprisingly, the exchange interaction follows the interatomic distances in the compounds with different crystal symmetry: $(\text{Nd}, \text{Tb})\text{Fe}_3(\text{BO}_3)_4$ and $\text{TbFe}_3(\text{BO}_3)_4$. The exception is for the exchange parameters at distances near 5.4 Å, which, in fact, couple the parallel spins.

At small distances the exchange interaction in $\text{TbFe}_3(\text{BO}_3)_4$ is stronger than the exchange interaction in $(\text{Nd}, \text{Tb})\text{Fe}_3(\text{BO}_3)_4$, which can be explained by the larger unit cell of the latter. However, at large distances, the exchange interaction converges to a close value (Fig. 6). Remarkably, this interaction remains rather strong and weakly depends on the distance. Probably, the overlap for super-exchange is more favourable in some cases, despite larger distances. However, the possibility of a “remanent” long-range dipole-dipole interaction, which is not taken into account in the exchange Hamiltonian, cannot be ruled out.

VII. CONCLUSIONS

The performed inelastic neutron scattering measurements in the ferrobates $\text{Nd}_{1-x}\text{Tb}_x\text{Fe}_3(\text{BO}_3)_4$ and $\text{TbFe}_3(\text{BO}_3)_4$, with the *easy-axis* magnetic structure reveal a rich picture of magnetic excitations up to ~ 6 meV.

There is a clear evolution of the magnetic excitation spectra upon the transition from the *easy-plane* (in Tb-free compound) to the *easy-axis* (in Tb-substituted compounds) magnetic structure. We conclude that every magnetic structure is characterized by hybridized Fe and R modes: quasicoustic and quasioptical (exchange) Fe branches, as well as Nd branches, which are determined by a Fe-Nd exchange splitting of the ground doublet Nd^{3+} . In the *easy-plane* structure, in

the vicinity of the Brillouin zone center, there are two pairs of different quasiaoustic Fe and Nd modes in contrast to the *easy-axis* state, where two corresponding branches are degenerated. The high-energy (exchange) branches are similar in both spin configurations. This is a consequence of the relatively weak anisotropic interactions compared to the isotropic Fe-Fe exchange.

The Ising character of the Tb³⁺ ion prevents the magnetic moment from precession. The Tb ions, possessing a maximum exchange Tb-Fe splitting in the *easy-axis* magnetic structure, change the effective magnetic anisotropy and stabilize the *easy-axis* state.

The spin-wave dispersion in Nd_{1-x}Tb_xFe₃(BO₃)₄ and TbFe₃(BO₃)₄ with similar magnetic structures, but with different crystal symmetry, strongly differ, most notably in the number of the spin wave branches due to the different crystal structure, SG *R*32 and *P*3₁21, respectively.

The application of a magnetic field perpendicular to the spins in the *easy-axis* state results in a splitting of the degenerated low-energy quasiaoustic Fe and Nd branches, caused by the imposed asymmetry in the basic plane, and in inducing of a spin canting.

It was established within a standard spin-wave theory approach that the main branches of the Fe and Nd subsystems are determined by similar values of Fe-Fe and Nd-Fe exchange parameters, both in the pure Nd- and in the Tb-doped compounds. The hierarchy of the different interactions was established. The Fe-Fe intrachain interactions are prevailing over the Fe-Fe interchain ones.

It was found that the value of the exchange parameters is slowly decreasing with increasing the interatomic distances and remains large at distances as extended as up to 7 Å.

ACKNOWLEDGMENTS

We are very grateful to Dr. A. Ivanov, Dr. D. Aristov, Dr. A. Mirmelstein, and Dr. E. Clementiev for fruitful discussions, which significantly expanded our understanding of the problem. The work was supported by the Russian Foundation for Basic Research (Grant No. 20-02-00109). A.A.M. acknowledges the financial support from the Russian Science Foundation (Grant No. 16-12-10531).

-
- [1] G. A. Smolenskii and I. E. Chupis, *Sov. Phys. Uspekhi* **25**, 475 (1982).
- [2] H. Schmid, *Ferroelectrics* **162**, 317 (1994).
- [3] J. A. Campá, C. Cascales, E. Gutiérrez-Puebla, M. A. Monge, I. Rasines, and C. Ruíz-Valero, *Chem. Mater.* **9**, 237 (1997).
- [4] J. E. Hamann-Borrero, M. Philipp, O. Kataeva, M. V. Zimmermann, J. Geck, R. Klingeler, A. Vasiliev, L. Bezmaternykh, B. Büchner, and C. Hess, *Phys. Rev. B* **82**, 094411 (2010).
- [5] A. A. Mukhin, A. M. Kuzmenko, V. Yu. Ivanov, A. G. Pimenov, A. M. Shuvaev, and V. E. Dziom, *Russ. Phys. – Usp.* **58**, 993 (2015).
- [6] A. A. Mukhin, G. P. Vorob'ev, V. Yu. Ivanov, A. M. Kadomtseva, A. S. Narizhnaya, A. M. Kuz'menko, Yu. F. Popov, L. N. Bezmaternykh, and A. Gudim, *JETP Lett.* **93**, 275 (2011).
- [7] A. M. Kadomtseva *et al.*, *Low Temp. Phys.* **36**, 511 (2010).
- [8] A. K. Zvezdin, S. S. Krotov, A. M. Kadomtseva, G. P. Vorob'ev, Yu. F. Popov, A. P. Pyatakov, L. N. Bezmaternykh, and E. A. Popova, *JETP Lett.* **81**, 272 (2005).
- [9] A. K. Zvezdin, G. P. Vorob'ev, A. M. Kadomtseva, Yu. F. Popov, P. Pyatakov, L. N. Bezmaternykh, A. V. Kuvardin, and E. A. Popova, *JETP Lett.* **83**, 509 (2006).
- [10] A. M. Kadomtseva, A. K. Zvezdin, A. P. Pyatakov, A. V. Kuvardin, G. P. Vorob'ev, Yu. F. Popov, and L. N. Bezmaternykh, *JETP* **105**, 116 (2007).
- [11] K.-C. Liang, R. P. Chaudhury, B. Lorenz, Y. Y. Sun, L. N. Bezmaternykh, V. L. Temerov, and C. W. Chu, *Phys. Rev. B* **83**, 180417(R) (2011).
- [12] F. Yen, B. Lorenz, Y. Y. Sun, C. W. Chu, L. N. Bezmaternykh, and A. N. Vasiliev, *Phys. Rev. B* **73**, 054435 (2006).
- [13] I. V. Golosovsky, A. I. Vasilev, A. A. Mukhin, E. Ressouche, V. Skumryev, I. Urcelay-Olabarria, I. A. Gudim, and L. N. Bezmaternykh, *Phys. Rev. B* **99**, 134439 (2019).
- [14] A. K. Zvezdin *et al.*, *JETP* **109**, 68 (2009).
- [15] J. Jeong *et al.*, *Phys. Rev. Lett.* **108**, 077202 (2012).
- [16] H. Ehrenberg, H. Weitzel, H. Fuess, and B. Hennion, *J. Phys.: Condens. Matter* **11**, 2649 (1999).
- [17] F. Ye, R. S. Fishman, J. A. Fernandez-Baca, A. A. Podlesnyak, G. Ehlers, H. A. Mook, Y. Wang, B. Lorenz, and C. W. Chu, *Phys. Rev. B* **83**, 140401(R) (2011).
- [18] X. Fabrèges, S. Petit, I. Mirebeau, S. Pailhès, L. Pinsard, A. Forget, M. T. Fernandez-Diaz, and F. Porcher, *Phys. Rev. Lett.* **103**, 067204 (2009).
- [19] T. Chatterji, *Pramana* **71**, 847 (2008).
- [20] D. Senff, P. Link, K. Hradil, A. Hiess, L. P. Regnault, Y. Sidis, N. Aliouane, D. N. Argyriou, and M. Braden, *Phys. Rev. Lett.* **98**, 137206 (2007).
- [21] S. Hayashida, M. Soda, S. Itoh, T. Yokoo, K. Ohgushi, D. Kawana, H. M. Rønnow, and T. Masuda, *Phys. Rev. B* **92**, 054402 (2015).
- [22] I. V. Golosovsky, A. K. Ovsyanikov, D. N. Aristov, P. G. Matveeva, A. A. Mukhin, M. Boehm, L.-P. Regnault, L. N. Bezmaternykh, *J. Magn. Magn. Mater.* **451**, 443 (2018).
- [23] A. M. Kuzmenko, A. A. Mukhin, V. Yu. Ivanov, A. M. Kadomtseva, and L. N. Bezmaternykh, *JETP Lett.* **94**, 294 (2011).
- [24] A. M. Kuzmenko, A. A. Mukhin, V. Y. Ivanov, and L. N. Bezmaternykh, *Solid State Phenomena* **190**, 269 (2012).
- [25] D. Fausti, A. A. Nugroho, and P. H. M. van Loosdrecht, S. A. Klimin, M. N. Popova, and L. N. Bezmaternykh, *Phys. Rev. B* **74**, 024403 (2006).
- [26] M. N. Popova, E. P. Chukalina, T. N. Stanislavchuk, B. Z. Malkin, A. R. Zakirov, E. Antic-Fidancev, E. A. Popova, L. N. Bezmaternykh, and V. L. Temerov, *Phys. Rev. B* **75**, 224435 (2007).
- [27] M. I. Kobets, K. G. Dergachev, E. N. Khatsko, S. L. Gnatchenko, L. N. Bezmaternykh, and V. L. Temerov, *Physica B* **406**, 3430 (2011).

- [28] I. A. Gudim, E. V. Eremin, and V. L. Temerov, *J. Crystal Growth* **312**, 2427 (2010).
- [29] <https://www.ill.eu/users/instruments/instruments-list/in12/characteristics/>.
- [30] P. Fisher *et al.*, *J. Phys.: Condens. Matter* **18**, 7975 (2006).
- [31] M. Janoschek, P. Fischer, J. Schefer, B. Roessli, V. Pomjakushin, M. Meven, V. Petricek, G. Petrakovskii, and L. Bezmaternikh, *Phys. Rev. B* **81**, 094429 (2010).
- [32] S. A. Klimin, D. Fausti, A. Meetsma, L. N. Bezmaternykh, P. H. M. van Loosdrecht, and T. T. M. Palstra, *Acta Crystallogr. B* **61**, 481 (2005).
- [33] C. Ritter, A. Balaev, A. Vorotynov, G. Petrakovskii, D. Velikanov, V. Temerov, and I. Gudim, *J. Phys.: Condens. Matter* **19**, 196227 (2007).
- [34] C. Ritter, A. Vorotynov, A. Pankrats, G. Petrakovskii, V. Temerov, I. Gudim, and R. Szymczak, *J. Phys.: Condens. Matter* **22**, 206002 (2010).
- [35] C. Ritter, A. Pankrats, I. Gudim, and A. Vorotynov, *J. Phys.: Conf. Ser.* **340**, 012065 (2012).
- [36] S. Tóth and S. Ward, spinw.org (2019).
- [37] F. Bloch, *Z. Phys.* **61**, 206 (1930).
- [38] J. C. Slater, *Phys. Rev.* **35**, 509 (1930).
- [39] S. Petit, *Collection Société Française de Neutrons* **12**, 105 (2011).
- [40] V. A. Bedarev, M. I. Paschenko, M. I. Kobets, K. G. Dergachev, E. N. Khatsko, S. L. Gnatchenko, A. A. Zvyagin, T. Zajarniuk, A. Szewczyk, M. U. Gutowska, L. N. Bezmaternykh, and V. L. Temerov, *Low Temp. Phys.* **41**, 534 (2015).
- [41] See Supplemental Material at <http://link.aps.org/supplemental/10.1103/PhysRevB.103.214412> for the raw spin-wave dispersion plots, without any treatment (smoothing).
- [42] D. Szaller, V. Kocsis, S. Bordács, T. Fehér, T. Rőöm, U. Nagel, H. Engelkamp, K. Ohgushi, and I. Kézsmárki, *Phys. Rev. B* **95**, 024427 (2017).
- [43] J. Goodenough, *Magnetism and the Chemical Bond* (Interscience Publishers, New York, 1963).